Acta Crystallographica Section A
Foundations of Crystallography
ISSN 0108-7673

Received 9 April 2004
Accepted 5 July 2004

Refinement of the crystal structural parameters of the intermediate phase of *h*-$BaTiO_3$ using convergent-beam electron diffraction

Yoichiro Ogata,[a]* Kenji Tsuda,[a] Yukikuni Akishige[b] and Michiyoshi Tanaka[a]

[a]Institute of Multidisciplinary Research for Advanced Materials, Tohoku University, Sendai 980-8577, Japan, and [b]Faculty of Education, Shimane University, Matsue 690-8504, Japan. Correspondence e-mail: ogata@mail.tagen.tohoku.ac.jp

Crystal structural parameters (21 positional parameters and nine isotropic Debye–Waller factors) of the intermediate phase of hexagonal barium titanate (*h*-$BaTiO_3$) have been refined by a structure analysis method using convergent-beam electron diffraction (CBED); this method was developed by Tsuda & Tanaka [*Acta Cryst.* (1999), A**55**, 939–954]. In order to perform the analysis, a parallel computation using a computer cluster composed of 16 connected Pentium 4 PCs was introduced. A function of parallel computation has been implemented in our analysis software, *MBFIT*, with the aid of the *Message Passing Interface* (*MPI*). Parallel computation enabled the present refinement to be conducted using a [001] CBED pattern and a [010] CBED pattern simultaneously. Reliable errors for the refined structural parameters have been obtained from the analyses of four independent experimental data sets instead of using the errors obtained by the error-propagation rule of least-squares fitting. The parameters obtained have been found to agree well with those determined by a neutron Rietveld analysis.

1. Introduction

In recent years, quantitative analyses of convergent-beam electron diffraction (CBED) data for the determination of atom positions and Debye–Waller factors have been performed by many researchers on the basis of the dynamical diffraction theory. According to the experimental data analysed, these analyses can be classified into the following four groups: integrated intensities of zeroth-order Laue-zone (ZOLZ) reflections (Jansen *et al.*, 1998; Yu *et al.*, 2000), line profiles of higher-order Laue-zone (HOLZ) reflections (Tanaka & Tsuda, 1990, 1991; Holmestad *et al.*, 1993; Tsuda & Tanaka, 1995; Nüchter *et al.*, 1998), two-dimensional intensities of ZOLZ reflections (Saunders *et al.*, 1999) and two-dimensional intensities of ZOLZ and HOLZ reflections (Tsuda & Tanaka, 1999; Tsuda *et al.*, 2002). The method described by Tsuda and co-workers (Tsuda & Tanaka, 1999; Tsuda *et al.*, 2002) is based on nonlinear least-squares fitting between energy-filtered experimental intensities of ZOLZ and HOLZ reflections and theoretical intensities calculated by the dynamical diffraction theory. The use of HOLZ reflections is essential for the method because those reflections with large reciprocal vectors are sensitive to small displacements of atoms. The method has the following advantages in contrast to the X-ray and neutron diffraction methods.

(i) *Nanometre-size crystal structure analysis*. CBED patterns can be obtained from specimen areas of a few nanometres in diameter. Thus, the CBED method enables us to conduct the structure determination of not only perfect crystals but also imperfect parts of crystals.

(ii) *Dynamical diffraction effect*. The CBED intensities contain phase information of crystal structure factors through the strong dynamical diffraction effect.

(iii) *Site-selective analysis*. Incident electrons form Bloch states in a specimen, also due to the strong dynamical diffraction effect, which are concentrated on specific atom rows. The use of the Bloch states allows site-selective structure analysis.

(iv) *High sensitivity to charge distributions*. Structure factors of low-order reflections for electron diffraction are more sensitive to the distributions of valence electrons than those for X-ray diffraction.

These are characteristic features of the CBED method only.

The use of two-dimensional intensity distributions of the reflections provides more information on structural parameters than the use of one-dimensional line profiles and improves the accuracy and reliability of the structure analysis. Energy filtering to remove inelastically scattered intensities, especially those due to plasmon excitation, is indispensable for quantitative analysis of CBED patterns. For this purpose, Tanaka and co-workers (Tsuno *et al.*, 1997; Tanaka *et al.*, 1998) developed a new energy-filter transmission electron microscope, JEM-2010FEF, which can take energy-filtered CBED patterns extending to a high angle of up to 10° at 100 kV,

which corresponds to $\sin\theta/\lambda \simeq 2.4$ Å^{-1}, with little distortion. Tsuda & Tanaka (1999) improved the previous analysis software so as to deal with the two-dimensional intensity data and to use the perturbation method, which was proposed by Peng & Cowley (1986), Bird (1990) and Zuo (1991), to obtain the eigenvalues of structure matrices for small changes of the structural parameters. Tsuda & Tanaka (1999) performed for the first time the refinement of crystal structural parameters using two-dimensional intensity distributions in the ZOLZ and HOLZ reflection discs of energy-filtered CBED patterns. One positional parameter and four anisotropic Debye–Waller factors of CdS (Tsuda & Tanaka, 1999) were refined. Subsequently, one positional parameter and eight anisotropic Debye–Waller factors of the rhombohedral phase of $LaCrO_3$ (Tsuda *et al.*, 2002) were refined.

Despite the introduction of the perturbation method, the analysis still needed long computation times for dynamical calculations. For this reason, the application of the method has so far been limited to crystals that possess few positional parameters to be refined. This limitation can be greatly eased by parallel computation. Recently, we have introduced a computer cluster composed of 16 connected Pentium 4 PCs (16-node Pentium 4 PC cluster), which works as a parallel computer, and have implemented a function of parallel computation in our analysis software, *MBFIT*, with the aid of the *Message Passing Interface* (*MPI*; Message Passing Interface Forum, 1995).

In the present paper, the crystal structural parameters of the intermediate phase of hexagonal barium titanate (h-$BaTiO_3$), which has 21 positional parameters and nine isotropic Debye–Waller factors to be determined, have been refined by the CBED structure analysis method using the PC cluster. The refinement was carried out by nonlinear least-squares fitting using [001] and [010] CBED patterns simultaneously to determine coordinates x, y and z at the same time. Reliable errors of refined structural parameters were obtained from the analyses of four independent experimental data sets instead of using the errors obtained by the error-propagation rule of least-squares fitting. The structural parameters obtained are compared with those determined by a neutron Rietveld analysis.

2. Experimental and analysis

2.1. Experimental

h-$BaTiO_3$ is one of the two polymorphic forms of barium titanate; the other is the well known cubic $BaTiO_3$. Fig. 1 shows the crystal structure of h-$BaTiO_3$ at room temperature; the crystal has six molecular units in the unit cell, with lattice parameters $a_h = 5.735$ and $c_h = 14.05$ Å, and belongs to space group $P6_3/mmc$ (Burbank & Evans, 1948). The figure was drawn with the *VENUS* software (Izumi & Dilanian, 2002).

Sawaguchi *et al.* (1985*a*,*b*) found that h-$BaTiO_3$ undergoes two successive phase transformations, at 222 and 74 K. Yamamoto *et al.* (1988) determined from an X-ray diffraction experiment that the intermediate phase between 222 and 74 K belongs to orthorhombic space group $C222_1$. From Raman (Yamaguchi *et al.*, 1987) and hyper-Raman (Inoue *et al.*, 1988) scattering experiments, the structural phase transformation at 222 K was found to be caused by condensation of the E_{2u} phonon mode at the Γ point.

Table 1
The atomic sites of the intermediate phase of h-$BaTiO_3$.

Site	Wyckoff position	Coordinate
Ba(1)	4*b*	$0, y, \frac{1}{4}$
Ba(2)	8*c*	x, y, z
Ti(1)	4*a*	$x, 0, 0$
Ti(2)	8*c*	x, y, z
O(1)	4*b*	$0, y, \frac{1}{4}$
O(2)	8*c*	x, y, z
O(3)	8*c*	x, y, z
O(4)	8*c*	x, y, z
O(5)	8*c*	x, y, z

The hexagonal axes of the room-temperature phase and the orthorhombic axes of the intermediate phase are related by $\mathbf{a}_o = \mathbf{a}_h$, $\mathbf{b}_o = \mathbf{a}_h + 2\mathbf{b}_h$ and $\mathbf{c}_o = \mathbf{c}_h$, where $\mathbf{a}_h$, $\mathbf{b}_h$ and $\mathbf{c}_h$ are the lattice parameters of the hexagonal lattice, and $\mathbf{a}_o$, $\mathbf{b}_o$ and $\mathbf{c}_o$ are those of the orthorhombic lattice. The atomic coordinates of the intermediate phase of h-$BaTiO_3$ are given in Table 1.

Single crystals of h-$BaTiO_3$ were grown from molten $BaTiO_3$ (Sawaguchi *et al.*, 1985*a*,*b*). Thin foil specimens for the CBED experiments were prepared by chemical polishing using phosphoric acid heated at ∼473 K. The CBED experiments were conducted using an energy-filter transmission electron microscope, JEM-2010FEF (Tanaka *et al.*, 1998). CBED patterns were taken with [001] and [010] incidences at a specimen temperature of 90 K using a liquid-nitrogen-cooled specimen holder. The intensities of the CBED patterns were recorded on imaging plates. The specimen thicknesses of the [001] and [010] CBED patterns for the first and second data sets were 470 and 540 Å, respectively, and the specimen

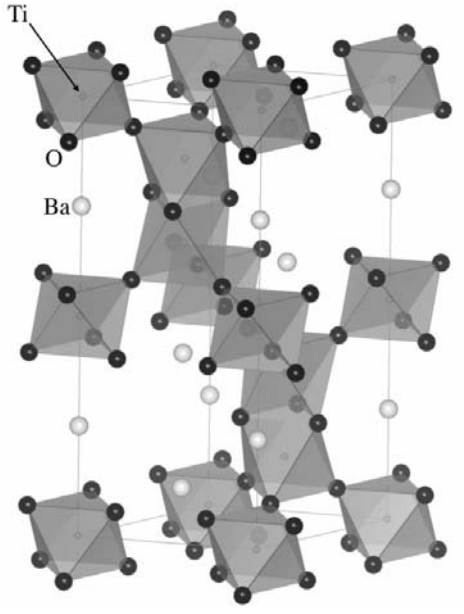

Figure 1
The crystal structure of h-$BaTiO_3$.

thicknesses of the [001] and [010] CBED patterns for the third and fourth data sets were 770 and 280 Å, respectively. The accelerating voltage of the electron microscope was determined to be 101.1 (2) kV from a HOLZ line pattern of silicon using the method described by Tsuda & Tanaka (1995).

Enantiomorphic twins exist in the intermediate phase. An enantiomorphic twin domain was carefully selected by examining the symmetries of the CBED patterns, although the domains cannot be distinguished using optical polarizing microscopes.

2.2. Analysis

According to the procedure described by Tsuda & Tanaka (1999), the distortions of the CBED patterns owing to the aberration of the lenses and the energy filter were corrected by assuming analytical expressions of the distortions. The remaining background intensities, due to thermal diffuse scattering (TDS), were subtracted by interpolating background intensities just outside a CBED disc in the radial direction. If Kikuchi lines or bands intersected a CBED disc, the intensities of the lines or bands were subtracted by linear interpolation between the background intensities just outside the disc along the lines or bands.

The structural parameters were refined by nonlinear least-squares fitting so as to minimize the residual sum of squares, χ^2, or the sum of squares of differences between the experimental CBED intensities and the theoretical ones. χ^2 is defined as

$$\chi^2 = \sum_i w_i [I_i^{\rm exp} - s I_i^{\rm cal}(\mathbf{r}, B)]^2, \qquad (1)$$

where $I_i^{\rm exp}$ is the ith experimental intensity, $I_i^{\rm cal}(\mathbf{r}, B)$ is the calculated intensity for atom positions $\mathbf{r}$ and Debye–Waller factors B, w_i is a weight factor and s is a scale factor common to all the calculated intensities. We set the weight factor $w_i = w_{\rm LZ}/(\sigma_i^{\rm exp})^2$, where $\sigma_i^{\rm exp}$ is the experimental error of $I_i^{\rm exp}$ and is evaluated as described by Tsuda & Tanaka (1999). $w_{\rm LZ}$ is an additional weight factor to decrease the weight of ZOLZ reflections in χ^2 according to the criterion described by Tsuda & Tanaka (1999) and also to equalize the contribution between the [001] pattern and the [010] pattern. Since intensities of ZOLZ reflections are much higher than those of HOLZ reflections and are insensitive to positional parameters, the weight of ZOLZ reflections should be decreased using $w_{\rm LZ}$. We have determined the values of $w_{\rm LZ}$ so as to satisfy two relations:

$$\sum_{\rm ZOLZ} w_i (I_i^{\rm exp})^2 \Big/ \sum_{\rm HOLZ} w_i (I_i^{\rm exp})^2 = 0.1 \qquad (2)$$

and

$$\sum_{[001]} w_i (I_i^{\rm exp})^2 = \sum_{[010]} w_i (I_i^{\rm exp})^2. \qquad (3)$$

The values of $w_{\rm LZ}$ for the first data set were $w_{\rm ZOLZ}^{[001]} = 0.021$, $w_{\rm HOLZ}^{[001]} = 1.0$, $w_{\rm ZOLZ}^{[010]} = 0.027$ and $w_{\rm HOLZ}^{[010]} = 0.11$. In the final step of fitting, the refinement was performed so as to minimize the total χ^2, $\chi^2_{\rm total} = \chi^2_{[001]} + \chi^2_{[010]}$, or the sum of χ^2 of [001] and [010] incidences. The nonlinear least-squares fitting was carried out using the analysis software *MBFIT* with the aid of parallel computation. The goodness of fit,

$$\mathrm{GOF} = [\chi^2/(N - M)]^{1/2}, \qquad (4)$$

was calculated, where N is the number of data points and M is the number of parameters to be refined.

Since the intensity at a point in the CBED pattern can be calculated independently of the intensity of the other points, the simulation of CBED intensities is suitable for parallel computation. Fig. 2 shows a schematic diagram of the parallel computation for CBED simulations. An attempt to perform CBED simulations on a parallel computer was reported by Birkeland *et al.* (1998). For parallel computation, we implemented communication routines of *MPI* in the analysis software *MBFIT*. In the present analysis, the CBED pattern was divided into 16 parts, and each part was calculated using each node of the 16-node Pentium 4 PC cluster. All the calculated parts were combined to form a complete CBED pattern.

3. Results

Fig. 3 shows energy-filtered CBED patterns obtained with [001] and [010] incidences at 90 K using the JEM-2010FEF electron microscope. The acceptance energy width was 0 ± 10 eV, and each pattern was obtained from a single domain area of a few nanometres in size. Each CBED pattern has twofold rotation symmetry. After the distortion correction and background subtraction, two-dimensional intensities of 94 reflections of the [001] pattern (Fig. 3*a*) and 110 reflections of the [010] pattern (Fig. 3*b*) were extracted. The numbers of total data points used were 301 646 for the [001] pattern and 212 380 for the [010] pattern. Each CBED pattern was divided into two parts, which are symmetrically equivalent because of the twofold symmetry, to create two independent experimental data sets for fitting. The first set combines one-half of the [001] pattern and one-half of the [010] pattern, *i.e.* 47 independent reflections (150 823 points) from the [001] pattern and 55 independent reflections (106 190 points) from the [010] pattern. The second set combines the other half of

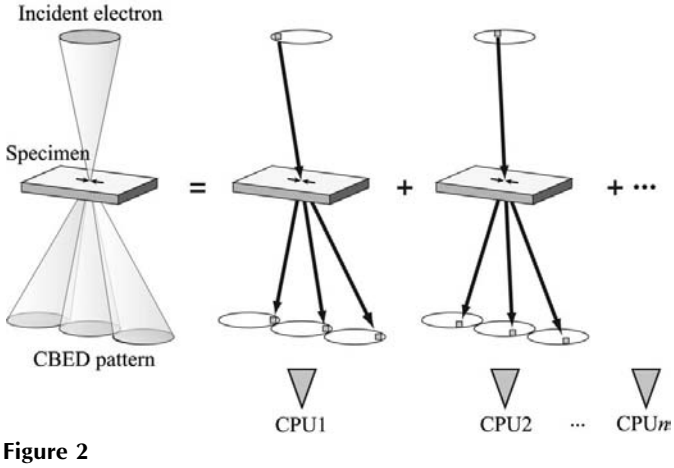

Figure 2
A schematic diagram of the parallel computation of a CBED pattern.

the [001] pattern and the other half of the [010] pattern. We took another set of energy-filtered [001] and [010] CBED patterns, extracted two-dimensional intensities from these patterns and subsequently created two further data sets. These four data sets were used for the fitting and evaluation of the standard deviations.

From the results of the convergence tests of calculated intensities with respect to the number of reflections for the first and second sets, 873 reflections were used for the dynamical calculations of the [001] pattern and 833 reflections for those of the [010] pattern. The parameters to be refined in the fitting were the positional parameters (fractional coordinates) listed in Table 1, isotropic Debye–Waller factors, specimen thicknesses $t_{[001]}$ and $t_{[010]}$, scale factors $s_{[001]}$ and $s_{[010]}$, and 204 geometrical parameters to adjust the positions of the reflection discs. The lattice parameters at 90 K used for the fitting were $a = 5.727$, $b = 9.890$Å and $c = 13.942$ Å (Akishige *et al.*, 1988). The atom positions of the high-temperature phase (Burbank & Evans, 1948) were used as initial values of the fitting. The nonlinear least-squares fitting was performed in the following steps in order to avoid the fitting from convergence to a pseudo-minimum. In the first step, the x and y coordinates and the isotropic Debye–Waller factors were refined using the [001] data. In the next step, the z coordinates were refined using the [010] data. In the final step, all the parameters were refined with the simultaneous use of the [001] and [010] data. Parallel computation using the PC cluster was applied to all the steps. For the fitting of the final step, parallel computation was indispensable, because the calculation time was decreased to about 7.5 h per cycle using parallel computing from five days per cycle when a single Pentium 4 PC was used.

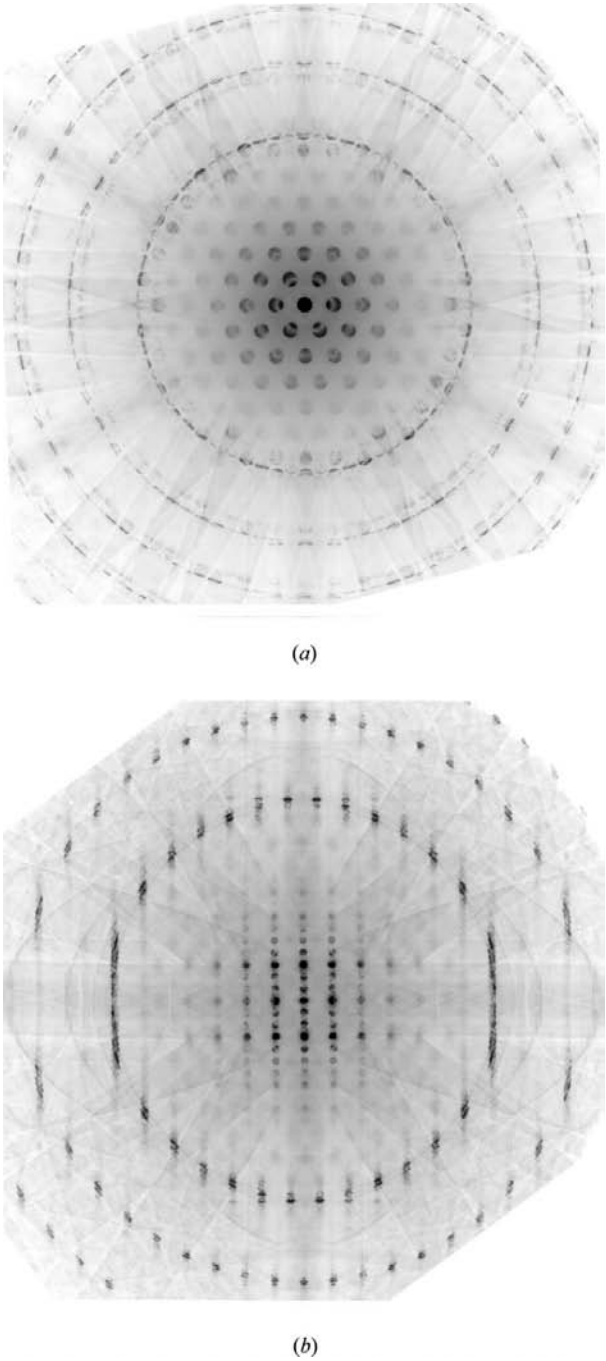

Figure 3
Energy-filtered CBED patterns of the intermediate phase of h-$BaTiO_3$, obtained with (*a*) [001] and (*b*) [010] incidence directions at 90 K.

The result of the fitting of CBED patterns for the first data set is shown in Fig. 4. The patterns in the left, centre and right columns, respectively, show experimental, calculated and difference patterns. The calculated patterns are seen to agree very well with the experimental patterns; the final GOF was 3.07. The refined values of the positional parameters and the Debye–Waller factors are given in the third column of Table 2; these are the average values of the four independent fits. The values in parentheses are the standard deviations of the refined parameters.

After the refinement, low-order structure factors were refined in order to obtain the charge-density distribution. We will discuss the charge-density distribution elsewhere.

4. Discussion

4.1. Evaluation of the standard deviations of the structural parameters

Standard deviations of crystal structural parameters are usually evaluated by the use of the error-propagation rule of least-squares fitting. However, in Rietveld refinements of X-ray and neutron diffraction using one-dimensional powder diffraction data, it was pointed out by Sakata & Cooper (1979) that the standard deviations are underestimated because of correlations between adjacent data points. Thus, in the present refinements using two-dimensional CBED patterns, the standard deviations are expected to be considerably underestimated, because the correlations between data points in two-dimensional CBED patterns are much higher.

In the present study, we carried out four independent fittings to determine reliable standard deviations of parameters to be refined using four independent experimental data sets. The standard deviations of the refined parameters in the four fittings were taken as the determination errors, which are

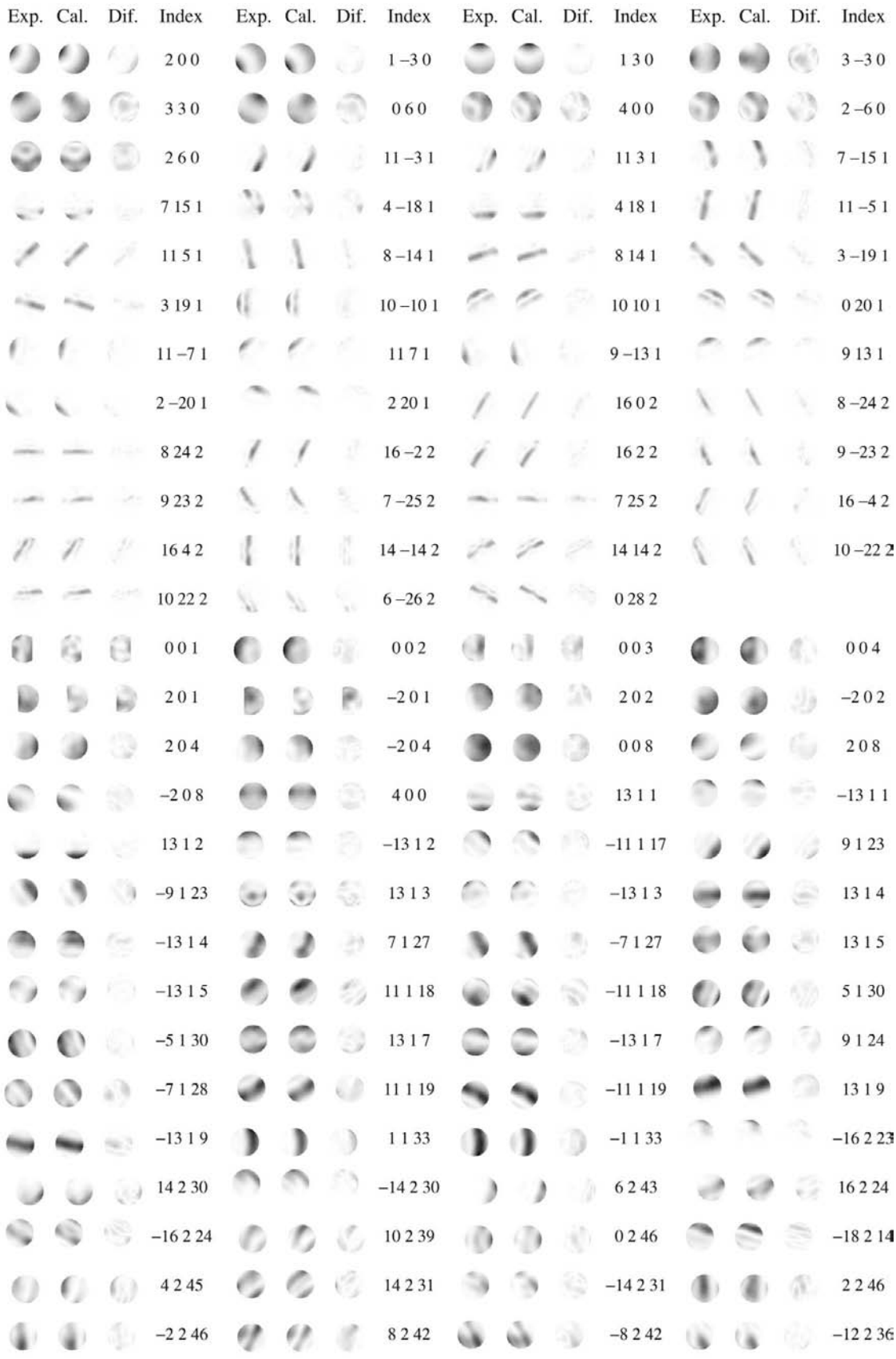

Figure 4
The result of the fitting of the CBED pattern of *h*-$BaTiO_3$. The patterns in the left, centre and right columns show, respectively, experimental, calculated and difference patterns.

given in parentheses in the third column of Table 2. For comparison, the refined parameters from the first data set and the standard deviations given by the error-propagation rule of least-squares fitting are shown in the fourth column of Table 2. The standard deviations determined from the four data sets appear to provide realistic errors of the CBED structure analysis method. Thus, it is evident that the error-propagation rule underestimates the errors in the present refinement using two-dimensional data with a large number of data points.

4.2. Comparison with the result of a neutron Rietveld analysis

The values of positional parameters and Debye–Waller factors obtained by a neutron Rietveld analysis at 150 K (Noda *et al.*, 1999; Akiyama, 1999) are shown in the fifth column of Table 2 for comparison. It is seen that the values agree well with the CBED values except for atoms Ba(2), Ti(1) and Ti(2). The standard deviations of the heavy Ba and Ti atoms determined by the present method are better than those obtained by the neutron Rietveld analysis, but those of the light O atoms, especially O(2), obtained by the present method are worse than those obtained by the neutron Rietveld analysis. The large standard deviations for atom O(2) originate from the fact that the values for the first and second data sets differ significantly from those for the third and fourth data sets. These large differences may have arisen by accident due to the specimen thicknesses at which the CBED patterns taken are insensitive to O(2), because the values of the other O atoms were determined with smaller standard deviations.

The standard deviations of the neutron study may be underestimated because the error propagation rule was applied. The neutron method can have an advantage in determining the positions of O atoms, because the neutron scattering factor for O atoms is larger than those for Ba and Ti atoms, but the electron scattering factor for O atoms is smaller than those for Ba and Ti atoms. There is a large difference in the numbers of data points between the CBED analysis and the neutron Rietveld analysis because the former uses two-dimensional data but the latter uses one-dimensional data. It is also noted that the maximum $\sin\theta/\lambda$ of the present analysis was 1.67 Å^{-1}, whereas that of the neutron Rietveld analysis was 0.83 Å^{-1}. Taking these facts into account, we can say that the accuracy and reliability of the CBED structure analysis are not worse than those of the neutron Rietveld analysis, even for the O atoms.

It is seen in Table 2 that there are differences between the x coordinates of atoms Ba(2), Ti(1) and Ti(2) of the present analysis and those of the neutron Rietveld analysis. The atomic displacements are reported to be explained by the atom-displacement pattern of the E_{2u} soft phonon mode of the high-temperature phase (Yamaguchi, 1987; Inoue *et al.*, 1988; Noda *et al.*, 1999; Akiyama, 1999). Fig. 5(*a*) shows the present

Table 2
Positional parameters and Debye–Waller factors (Å^2) of the intermediate phase of *h*-$BaTiO_3$.

Refined values at 90 K are given in the third column. In the fourth column, the values obtained by CBED analysis and the standard deviations estimated by the error-propagation rule of least-squares fitting are shown for comparison. The values obtained by a neutron Rietveld analysis at 150 K (Noda *et al.*, 1999; Akiyama, 1999) are shown in the right-hand column for comparison.

Site		CBED (Present result) 90 K	CBED (The first set) 90 K	Neutron diffraction 150 K
Ba(1)	x	0	0	0
	y	0.0004 (3)	0.000690 (5)	−0.0008 (8)
	z	0.25	0.25	0.25
	B	0.17 (1)	0.1621 (2)	0.15 (3)
Ba(2)	x	0.0095 (5)	0.008969 (4)	0.0055 (14)
	y	0.3338 (1)	0.333667 (5)	0.3333 (6)
	z	0.0964 (1)	0.096524 (1)	0.0969 (1)
	B	0.25 (1)	0.2378 (2)	0.33 (2)
Ti(1)	x	0.0206 (7)	0.02101 (2)	0.0170 (20)
	y	0	0	0
	z	0	0	0
	B	0.23 (4)	0.2007 (5)	0.42 (8)
Ti(2)	x	0.0155 (11)	0.01465 (1)	0.0130 (16)
	y	0.3326 (2)	0.332675 (9)	0.3294 (8)
	z	0.8459 (7)	0.846359 (3)	0.8457 (2)
	B	0.26 (4)	0.2715 (6)	0.33 (5)
O(1)	x	0	0	0
	y	0.5145 (4)	0.51403 (3)	0.5188 (6)
	z	0.25	0.25	0.25
	B	0.42 (7)	0.448 (1)	0.47 (7)
O(2)	x	0.7739 (30)	0.77101 (2)	0.7747 (6)
	y	0.7402 (40)	0.73756 (2)	0.7421 (4)
	z	0.2547 (37)	0.25734 (2)	0.2484 (6)
	B	0.43 (6)	0.3631 (8)	0.44 (4)
O(3)	x	0.0048 (11)	0.00544 (2)	0.0033 (16)
	y	0.8318 (9)	0.83050 (2)	0.8342 (5)
	z	0.0804 (18)	0.07903 (1)	0.0801 (5)
	B	0.57 (17)	0.438 (1)	0.34 (5)
O(4)	x	0.7510 (7)	0.75121 (3)	0.7477 (11)
	y	0.5799 (7)	0.57906 (2)	0.5851 (8)
	z	0.0759 (5)	0.07658 (3)	0.0794 (5)
	B	0.60 (13)	0.565 (2)	0.31 (10)
O(5)	x	0.2486 (19)	0.24883 (3)	0.2553 (12)
	y	0.5843 (12)	0.58314 (1)	0.5824 (9)
	z	0.0796 (22)	0.08113 (2)	0.0822 (5)
	B	0.55 (15)	0.520 (2)	0.42 (10)

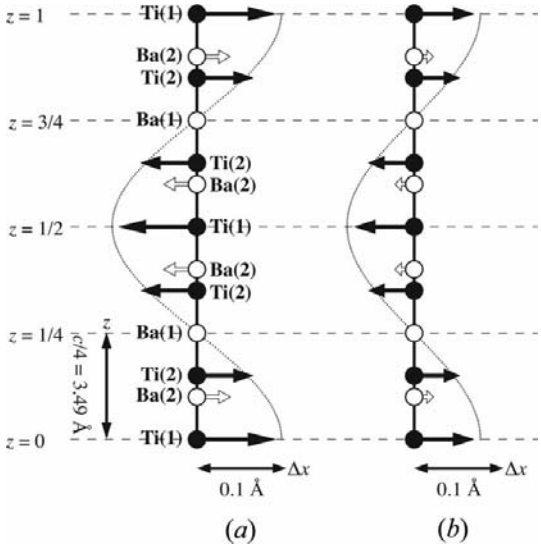

Figure 5
Atomic displacements of the intermediate phase of *h*-$BaTiO_3$, caused by phase transformation from the high-temperature phase. (*a*) Present result at 90 K and (*b*) neutron Rietveld analysis at 150 K (Noda *et al.*, 1999; Akiyama, 1999).

result of the atom displacements of the Ba and Ti atoms from the high-temperature phase, where the displacements of the Ti atoms are approximated by a sinusoidal envelope curve. Fig. 5(*b*) shows the atom displacements of the Ba and Ti atoms obtained by the neutron Rietveld analysis for comparison. The atom-displacement patterns of the present analysis and the neutron Rietveld analysis are similar but different in magnitude. The differences of the magnitudes of the atom displacements may be explained by the difference in the experimental temperatures, that is, the displacement Δx can be approximately expressed by $\Delta x \propto (T_c - T)^{1/2}$, where T_c is the transformation temperature 222 K and T is the experimental temperature. The experimental temperature of the present analysis was 90 K and that of the neutron Rietveld analysis was 150 K. Thus, the ratio of Δx between the analyses is expected to be

$$\Delta x^{(\text{present})}/\Delta x^{(\text{neutron})} = (T_c - 90)^{1/2}/(T_c - 150)^{1/2} = 1.35.$$

From the refined values of the x coordinates of atoms Ba(2), Ti(1) and Ti(2), the ratios are $\Delta x^{(\text{present})}_{\text{Ba(2)}}/\Delta x^{(\text{neutron})}_{\text{Ba(2)}} = 1.7\,(5)$, $\Delta x^{(\text{present})}_{\text{Ti(1)}}/\Delta x^{(\text{neutron})}_{\text{Ti(1)}} = 1.2\,(2)$ and $\Delta x^{(\text{present})}_{\text{Ti(2)}}/\Delta x^{(\text{neutron})}_{\text{Ti(2)}} = 1.2\,(2)$. These ratios agree with the expected value of 1.35 within the errors. Thus, we can say that the present result for the displacements of Ba and Ti atoms agrees with the result of the neutron Rietveld analysis when the experimental temperatures are taken into account and the condensation of the E_{2u} soft phonon mode is assumed.

5. Concluding remarks

We have applied the CBED structure analysis method developed by Tsuda & Tanaka (1999) to the analysis of the intermediate phase of *h*-$BaTiO_3$, which has 30 parameters to be refined. The refinement was carried out by nonlinear least-squares fitting using [001] and [010] CBED patterns simultaneously, in order to determine coordinates x, y and z at the same time. The present analysis was not possible until we introduced parallel computation, because a long calculation time was required. Parallel computation is crucial for the determination of crystal structures with many parameters. Parallel computation also raises the possibility of the analysis of local structures of imperfect crystals, which requires the use of a low-symmetry space group and a superlattice cell. For this purpose, a computer cluster with more components and faster computation capability is preferable. It is hoped that efforts to decrease the number of experimental data points without sacrificing the accuracy of the analysis will be made.

We have succeeded in the analysis from a single domain area of enantiomorphic twin domains using the features of nanometre-size analysis. A nanometre scale probe investigated with the CBED method has great advantages and can be used extensively. For example, perovskites and related materials with strongly correlated electrons are good targets, in which very small domains of twin structures exist and characteristic phase separation occurs easily.

The authors are grateful to Mr F. Sato for his careful maintenance of the JEM-2010FEF and to Professor M. Terauchi for stimulating discussions. KT acknowledges financial support from the Kazato Research Foundation. The present study was partly supported by Grants-in-Aid of Scientific Research from the Japan Society for the Promotion of Science.

References

Akishige, Y., Oomi, G. & Sawaguchi, E. (1988). *Solid State Commun.* **65**, 621.
Akiyama, K. (1999). Masters thesis, Chiba University, Japan. (In Japanese.)
Bird, D. M. (1990). *Acta Cryst.* A**46**, 208–214.
Birkeland, C., Holmestad, R., Marthinsen, K. & Høier, R. (1998). *J. Sci. Comput.* **13**, 1–18.
Burbank, R. D. & Evans, H. T. Jr (1948). *Acta Cryst.* **1**, 330–336.
Holmestad, R., Weickenmeier, A. L., Zuo, J. M., Spence, J. C. H. & Horita, Z. (1993). *Inst. Phys. Conf. Ser.* **138**, 141.
Inoue, K., Hasegawa, A., Watanabe, K., Yamaguchi, H., Uwe, H. & Sakudo, T. (1988). *Phys. Rev. B*, **38**, 6352–6355.
Izumi, F. & Dilanian, R. A. (2002). *Recent Research Developments in Physics*, Vol. 3, Part II, pp. 699–726. Trivandrum, India: Transworld Research Network.
Jansen, J., Tang, D., Zandbergen, H. W. & Schenk, H. (1998). *Acta Cryst.* A**54**, 91–101.
Message Passing Interface Forum (1995). *Message Passing Interface Standard.* Version 1.1. http://www.mpi-forum.org/docs/docs.html.
Noda, Y., Akiyama, K., Shobu, T., Kuroiwa, Y. & Yamaguchi, H. (1999). *Jpn J. Appl. Phys. Suppl.* **38-1**, 73–76.
Nüchter, W., Weickenmeier, A. L. & Mayer, J. (1998). *Acta Cryst.* A**54**, 147–157.
Peng, L.-M. & Cowley, J. M. (1986). *Acta Cryst.* A**42**, 545–552.
Sakata, M. & Cooper, M. J. (1979). *J. Appl. Cryst.* **12**, 554–563.
Saunders, M., Fox, A. G. & Midgley, P. A. (1999). *Acta Cryst.* A**55**, 480–488.
Sawaguchi, E., Akishige, Y. & Kobayashi, M. (1985*a*). *J. Phys. Soc. Jpn*, **54**, 480–482.
Sawaguchi, E., Akishige, Y. & Kobayashi, M. (1985*b*). *Jpn J. Appl. Phys. Suppl.* **24-2**, 252.
Tanaka, M. & Tsuda, K. (1990). *Proceedings of the 12th International Congress on Electron Microscopy*, edited by L. D. Peachy & D. B. Williams, Vol. 2, pp. 518–519. San Francisco Press.
Tanaka, M. & Tsuda, K. (1991). *Microbeam Analysis*, edited by D. G. Howitt, pp. 145–146. San Francisco Press.
Tanaka, M., Tsuda, K., Terauchi, M., Tsuno, K., Kaneyama, T., Honda, T. & Ishida, M. (1998). *J. Microsc.* **194**, 219–227.
Tsuda, K., Ogata, Y., Takagi, K., Hashimoto, T. & Tanaka, M. (2002). *Acta Cryst.* A**58**, 514–525.
Tsuda, K. & Tanaka, M. (1995). *Acta Cryst.* A**51**, 7–19.
Tsuda, K. & Tanaka, M. (1999). *Acta Cryst.* A**55**, 939–954.
Tsuno, K., Kaneyama, T., Honda, T., Tsuda, K., Terauchi, M. & Tanaka, M. (1997). *J. Electron Microsc.* **46**, 357–368.
Yamaguchi, H. (1987). Doctoral thesis, Tsukuba University, Japan. (In Japanese.)
Yamaguchi, H., Uwe, H., Sakudo, T. & Sawaguchi, E. (1987). *J. Phys. Soc. Jpn*, **56**, 589–595.
Yamamoto, T., Akishige, Y. & Sawaguchi, E. (1988). *J. Phys. Soc. Jpn*, **57**, 3665–3667.
Yu, R. C., Yakimansky, A. V., Kothe, H., Voigt-Martin, I. G., Schollmeyer, D., Jansen, J., Zandbergen, H. & Tenkovtsev, A. V. (2000). *Acta Cryst.* A**56**, 436–450.
Zuo, J. M. (1991). *Acta Cryst.* A**47**, 87–95.